DOI: https://doi.org/10.1007/s11071-024-09766-7

Energy function, hidden and self-excited firing activities of an improved Rulkov neuron, and its application in information patterns

Zeric Tabekoueng Njitacke [1], Clovis Ntahkie Takembo [1], Godwin Sani [2], Norbert Marwan [3], R. Yamapi[4], Jan Awrejcewicz[2]

[1]Department of Electrical and Electronic Engineering, College of Technology (COT), University of Buea, P.O.Box 63, Buea (Cameroon)

[2]Department of Automation, Biomechanics and Mechatronics, Lodz University of Technology, ul. Stefanowskiego 1/15, 90-537 Lodz, Poland

[3]Potsdam Institute for Climate Impact Research (PIK), Member of the Leibniz Association, Telegraphenberg, P.O. Box 601203, 14473 Potsdam, Germany

[4] Fundamental Physics Laboratory, Physics of Complex System group, Department of Physics, Faculty of Science, University of Douala, Box 24 157 Douala, Cameroon

Corresponding author

Zeric Njitacke Tabekoueng; email: zerictabekoueng@yahoo.fr; phone : +237670310325

Abstract:

Information patterns in a neuron model describe the possible modes in which information is processed and transmitted within neurons and neural networks. An improved Rulkov neuron is introduced and investigated, with possible application to information coding carried out in this work. After providing the neuron's empirical model, its stability around the single equilibrium point is examined, and it is discovered that the system is able to exhibit both stable and unstable dynamics. Using two-parameter charts, the system's global stability dynamics are obtained, and windows of the hidden and self-excited dynamics involving both chaotic and periodic states are clearly separated. For the validation of the result of the mathematical model, an electronic circuit was developed in Pspice simulation environment, and both results were in good accord. Finally, a network of 500 Rulkov neurons under the chain configuration is used to explore the phenomenon of the information patterns. From that investigation, it was found that the Rulkov network lattice is able to present repetitive, regular stripes of bright and dark bands that are almost periodic and localized in space and time.

Keywords: Continuous Rulkov neuron, Hidden and Self-excited dynamics, Energy proportions, Neural circuit, Information patterns.

1- Introduction

Information patterns in a neuron model describe the possible modes in which information is processed and transmitted within a neuron [1, 2]. This includes the patterns of electrical activity, such as action potentials and synaptic transmission, that enable neurons to communicate with each other and process sensory input [3]. These patterns are essential for understanding how neurons function and how information is encoded and transmitted in the brain. Studying these patterns can provide insights into how neural networks process information and contribute to our understanding of brain function and cognition [2, 4, 5]. That information pattern is addressed through the mastering of the behavior of the neuron used as a prototype. In general, neuron models are divided into two categories: discrete and continuous models.

Concerning the discrete neuron model, several studies have been done. In the work of ref. [6], the authors investigated a 2D map-based Rulkov neuron model. In their study, neural behaviors such as bursting and spiking were found. Using 18 MOS transistors, the circuit of the model was designed and then used to further support their study. Based on the random disturbance, a 1D Rulkov neuron model has been investigated in ref. [7]. As a result, the author was able to find under stochastic effect phenomena such as bursting, spiking, and bistability. Using a discrete memristor as a field-generating source, the magnetic effect has been investigated on the behavior of a Rulkov neuron in ref. [8]. From their study, the authors discovered that the model was able to experience long transient behaviors with the occurrence of chaotic bursting and hyperchaotic firing. An improved discrete Rulkov neuron with sine memductance was introduced in ref. [9]. Period doubling bifurcation and the coexistence of an infinite number of patterns of the same shape due to initial conditions boosting were reported in their work. In ref.[10], a local active discrete memristor was proposed. Afterward, it was coupled to the Rulkov neuron model to design a memristive version. The memristive version was therefore coupled to build a network. From the investigations of the coupled neurons, phenomena such as synchronization transition, phase synchronization, and coexistence of synchronization were reported.

Interesting contributions have also been made to the study of continuous models of neurons. As an example, a non-autonomous memristive Rulkov neuron model was suggested and studied in ref. [11]. From the study of the authors, they found that the model experienced a line of equilibrium from extreme multistable behavior, and their results were further validated using an electronic circuit realization of the neuron model. Taking as a drawback the fact that the electronic circuit of the continuous Rulkov neuron introduced in ref. [11] was made up of analog multipliers, which are a bit expensive, an improved memristive non-autonomous Rulkov neuron model was introduced in ref. [12]. After the investigation of the boundedness and stability of the equilibria, the authors used numerical simulations to show a variety of nonlinear behaviors in the model, amongst them is the extreme multistable phenomena. Based on a Helmholtz theorem, the Hamilton function was also proposed by the authors to discuss the energy released during each firing activity. Finally, a multiplier-less analog electronic circuit for the model was designed to validate their results.

From the quoted work, phenomena such as self-excited dynamics, hidden dynamics, coexisting patterns, complex behavior involving bursting and spiking, energy analysis, and information patterns were reported in some of the studied neurons. As it can be seen from the literature, fewer works are devoted to either the discrete or continuous Rulkov neuron model in comparison to popular neuron models such as the FitzHugh-Nagumo (FHN) neuron [13-16], the Hindmarsh-Rose (HR) neuron [17-19], or the Hodgkin-Huxley (HH) neuron [20-22]. This is why in this contribution, from the continuous memristive non-autonomous Rulkov neuron model introduced in ref.[12], an improved 2D non-autonomous memristor-less Rulkov neuron is proposed. From that model, striking properties of hidden and self-excited dynamics will be highlighted, including the energy proportion of the ion channel as well as the membrane potential. This study investigate the hysteretic dynamics of the model in order to reveal the windows of coexisting patterns, build an analog electronic circuit for the validation of the model, and finally, show that the continuous Rulkov neuron model is interesting for the investigation of information patterns via the powerful modulational instability theory.

To achieve this objective, the rest of the paper's contribution is organized as follows: Section 2 introduces the properties of the non-autonomous memristor-less Rulkov neuron model, such as the equilibrium point stability and the energy functions of the model. In Section 3, numerical simulations are used to characterize the dynamical behaviors of the model. The circuit implementation of the model and the chain network of 500 neurons used to predict possible information patterns are discussed in Section 4. The conclusion and the perspective of a future work are given in Section 5.

2- Analysis of the improved Rulkov neuron

2-1- Model and its features

The Rulkov neuron model is a mathematically structured model used to mimic the behavior of biological neurons in the brain. It was proposed in its discrete form in the work of Nikolai F. Rulkov[23]. The model is based on the idea that neurons are complex systems that can exhibit chaotic behavior, and it aims to capture the essential features of this behavior in a simple mathematical form. The Rulkov neuron model is composed of a set of differential equations that describe the dynamics of a single neuron. The equations take into account the effects of ion channels, membrane potentials, and other factors that influence the behavior of neurons. The model can be used to simulate the firing patterns of neurons under different conditions, and it has been used in a wide range of applications, from neuroscience research to the development of artificial neural networks. Very recently, based on some mathematical manipulation, a continuous memristive version of the Rulkov neuron was introduced in refs.[11, 12]. Based on the quoted work, an improved 2D non-autonomous Rulkov neuron is introduced in Eq. (1) of this work for which x represents the membrane potential and u recovery variable of the model.

$$\begin{cases} \dot{x} = \alpha\left(-\tanh\left(0.5|x|\right)+1\right)-x+u+i_m\sin\left(2\pi f\tau\right) \\ \dot{u} = -\beta x-\sigma \end{cases} \tag{1}$$

The equilibrium points of the proposed Rulkov neuron are obtained by solving the equations $\dot{x}=\dot{u}=0$; therefore after some mathematical manipulations, Eq. (2) is obtained

$$P\left(\bar{x};\bar{u}\right)=P\left(-\frac{\sigma}{\beta};\alpha\beta\tanh\left(0.5\left|\frac{\sigma}{\beta}\right|\right)-\alpha\beta-\sigma-i_m\beta\sin\left(2\pi f\tau\right)\right) \tag{2}$$

For the stability analysis, Eq. (1) is linearized around the equilibrium points $P\left(\bar{x};\bar{u}\right)$ and the Jacobian matrix of Eq. (3) is obtained.

$$J=\begin{bmatrix} -0.5\alpha\left(1-\tanh\left(0.5|\bar{x}|\right)^2\right)\frac{\bar{x}}{|\bar{x}|}-1 & 1 \\ -\beta & 0 \end{bmatrix} \tag{3}$$

Since the Jacobian matrix depend only on the Equilibrium point $\bar{x}$, exploiting its value given in Eq. (2), the model's characteristic equation is given in Eq. (4) by solving $\psi\left(\eta\right)=\det\left(J-\eta I\right)=0$

.

$$\eta^2+\left(1-0.5\alpha\tanh\left(0.5|\bar{x}|\right)^2\frac{\bar{x}}{|\bar{x}|}+0.5\alpha\frac{\bar{x}}{|\bar{x}|}\right)\eta+\beta=0 \tag{4}$$

From equation Eq. (4), the stability of the model will be discussed under the condition $\left(1-0.5\alpha\tanh\left(0.5|\bar{x}|\right)^2\frac{\bar{x}}{|\bar{x}|}+0.5\alpha\frac{\bar{x}}{|\bar{x}|}\right)>0$ since $\beta>0$.

Therefore, the system's stability situation with respect to the variation of the control parameter σ is presented in Table 1.

Table 1: Eigenvalues and the related stability for some discrete value of the parameter σ of the neuron model when $i_m=1$, $f=1$, $\alpha=10$ and $\beta=5$.

Parameter σ	Eigenvalues	Related stability
-1	$-1.737\pm1.407i$	Stable
-0.5	$-1.746\pm1.395i$	Stable
-10^{-3}	$-1.749\pm1.391i$	Stable
10^{-3}	$0.749\pm2.106i$	unstable
0.5	$0.746\pm2.107i$	unstable
1	$0.737\pm2.111i$	unstable

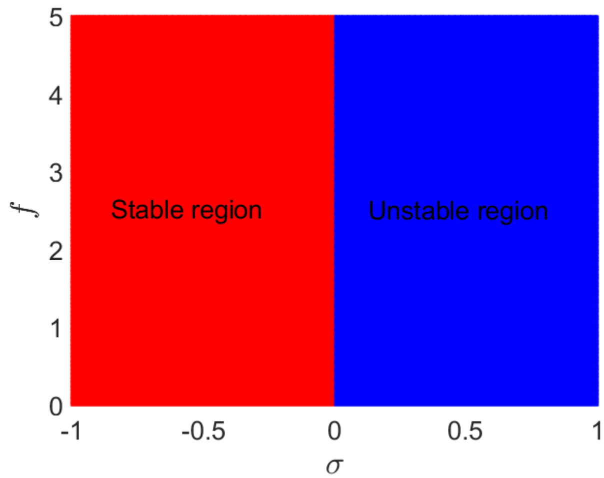

Fig.1: Two-parameters charts showing windows in which the model displays either stable or unstable dynamics, for the variation of σ and f when $i_m=1$, $\alpha=10$ and $\beta=5$.

2-2- Energy function of the Rulkov neuron

In this section, the objective is to establish the energy function of the Rulkov neuron, which consists of the energy of the neuron's membrane potential and the energy of its ion channels. In that way, the energy proportion of the membrane potential and that of the ion channels will be obtained compared to the total energy of the model.

To achieve our goal, let us express Eq. (1) as the sum of a conservative and dissipative vector field as follows [24]:

$$\begin{pmatrix} \dot{x} \\ \dot{u} \end{pmatrix} = \begin{pmatrix} u \\ -\beta x \end{pmatrix} + \begin{pmatrix} \alpha\left(-\tanh\left(0.5|x|\right)+1\right) - x + i_m \sin\left(2\pi f \tau\right) \\ -\sigma \end{pmatrix} = F_c + F_d \tag{5}$$

From Eq. (5), a Hamilton energy function of the considered Rulkov neuron is a solution of Eq. (6).

$$\nabla H^T f_c\left(x,u\right) = u\frac{\partial H}{\partial x} + \left(-\beta\right)\frac{\partial H}{\partial u} = 0 \tag{6}$$

Therefore a Hamilton function solution of Eq. (6) is provided as:

$$H = H_1 + H_2 = \frac{1}{2}x^2 + \frac{1}{2\beta}u^2 \tag{7}$$

To ensure the reliability of Hamilton's energy, some properties of the Helmholtz theorem [24] presented from Eq. (8) to Eq. (10) have to be verified:

$$\nabla H^T f_d\left(x,u\right) = \frac{dH}{d\tau} = \dot{H} = x\left(\alpha\left(-\tanh\left(0.5|x|\right)+1\right) - x + i_m \sin\left(2\pi f \tau\right)\right) - \frac{1}{\beta}u\sigma \tag{8}$$

After which the conservative and dissipative vector fields are expressed in terms of a skew symmetric matrix $J\left(x,u\right)$, a symmetric matrix $R\left(x,u\right)$ and the gradient vector field $\nabla H\left(x,u\right)$ as shown in Eqs. (9) and (10):

$$F_c = \begin{pmatrix} 0 & \beta \\ -\beta & 0 \end{pmatrix}\begin{pmatrix} x \\ \frac{u}{\beta} \end{pmatrix} = J\left(x,u\right)\nabla H \tag{9}$$

$$F_d = \begin{pmatrix} \frac{\alpha\left(-\tanh\left(0.5|x|\right)+1\right) - x + i_m \sin\left(2\pi f \tau\right)}{x} & 0 \\ 0 & \frac{-\beta\sigma}{u} \end{pmatrix}\begin{pmatrix} x \\ \frac{u}{\beta} \end{pmatrix} = R\left(x,u\right)\nabla H \tag{10}$$

Based on the Helmholtz theorem, the dimensionless Hamilton energy *H for* the Rulkov neuron meets all the necessary conditions for its validation. As it can be seen in Eq. (7), the energy function

H is made up of the superposition of the two components namely H_1 and H_2 representing respectively the energy provided by the membrane potential and the ion channels. Therefore, the energy contribution of the membrane potential can be given as $P_1 = \frac{H_1}{H}$ while the contribution of the ions channels is given by $P_2 = \frac{H_2}{H}$.

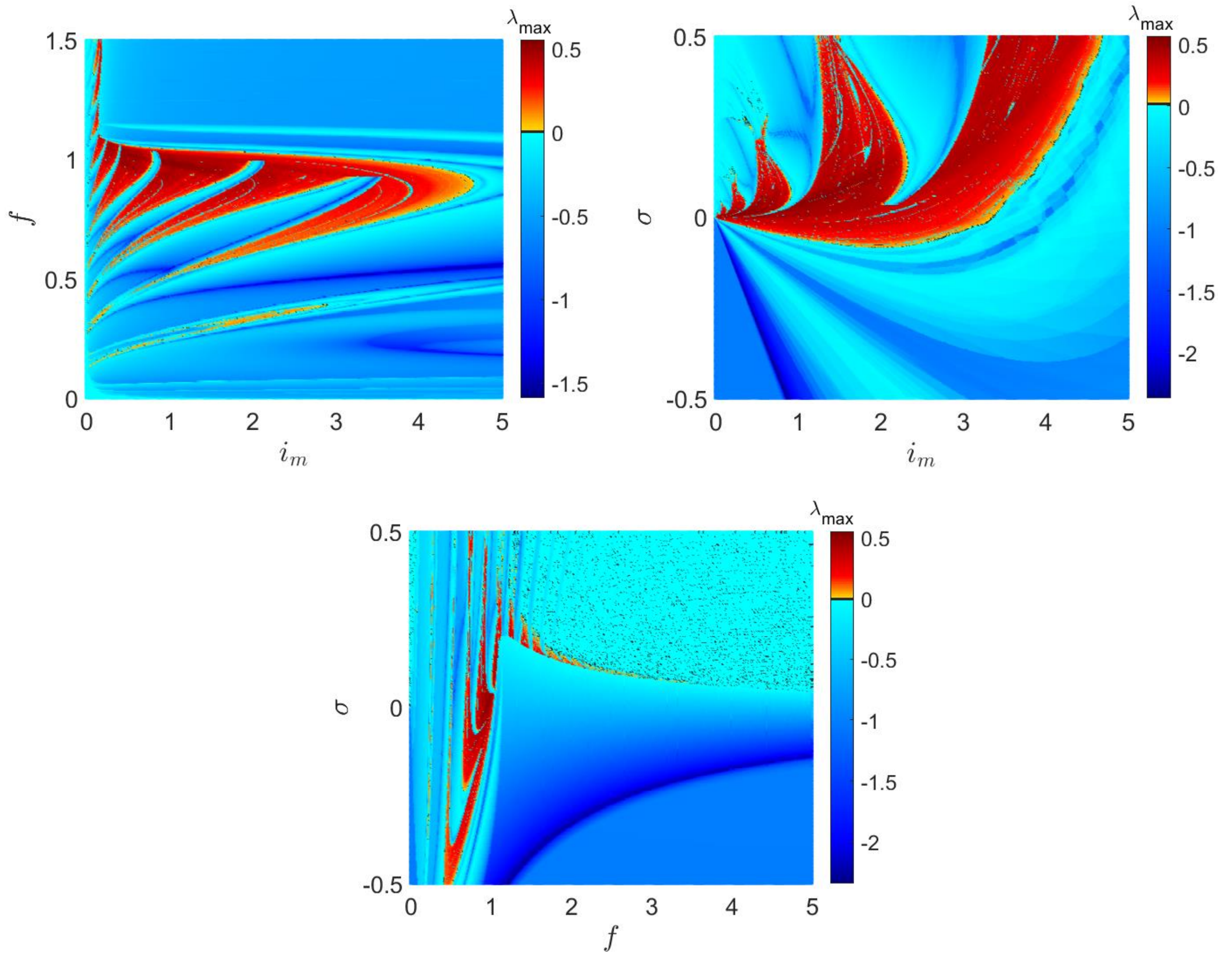

Fig.2: Two-parameter charts showing the global behavior of the improved Rulkov neuron model. The plane (i_m, f) is obtained for $\sigma = 0.03$; the plane (i_m, σ) is obtained for $f = 1$ and the The plane (f, σ) is obtained for $i_m = 1$. All these charts are computed using a continuation technique with ab initial starting point of $(-0.2, -0.02)$.

3. Numerical findings

Numerical investigations are carried out in this contribution using the well-known fourth-order Runge-Kutta computational algorithm, with selected parameters in extended precision mode. In addition, fixed-step time size of 5×10^{-3} is used for the accuracy of the integrations.

3.1 Two-parameter charts

In this section, some two-parameter charts are computed and used for characterizing the dynamical behavior of the considered neuron model. For example, Fig. 1 is computed under the variation of the external frequency source and the parameter σ. It is exploited to discuss the various ranges of parameters in which the model displays a stable (red) or an unstable behavior (blue). That diagram is of particular interest since it enables us to easily identify the windows of parameters in which either hidden or self-excited dynamics can occur in the model. In order to get an idea of the windows in which the model can exhibit either chaotic $(\lambda_{\max}>0)$ or periodic $(\lambda_{\max}<0)$ firing activities, the two-parameter charts (Fig. 2) have been computed, exploiting the sign of the maximum Lyapunov exponent. In the various planes considered for the studied Rulkov neuron, the windows of periodic behaviors are predominant compared to the chaotic behaviors. More importantly, in the planes (i_m,σ) and (f,σ) windows of hidden $(\sigma<0)$ and self-excited $(\sigma>0)$ dynamics can be easily identified based on the values and the sign of the parameter σ. In this particular case, hidden dynamics will be related to the firing activities coming from a stable equilibrium point, while self-excited firing activities will be related to the firing activities coming from an unstable equilibrium point.

3.2 One-parameter diagrams

Both the Lyapunov exponent and the bifurcation diagram are quantitative metrics used for characterizing chaos. The bifurcation diagram shows the qualitative changes in the behavior of a neuron as a parameter is varied, while the Lyapunov exponent estimates the rate of divergence of nearby trajectories in phase space. Both of these metrics provide quantitative information about the dynamics of a neural system and can be used to analyze and predict its behavior. Therefore, they are not just qualitative metrics but also quantitative metrics. In this contribution, three main coefficients namely, the parameter σ, the amplitude i_m and the frequency f of the external excitation are used as bifurcation control parameters as shown in Fig.3. When varying the control parameter σ as can be seen in Fig. 3a, two main types of dynamical regimes can be recorded: the self-excited dynamics with $(\sigma > 0)$ and the hidden dynamics with $(\sigma < 0)$.

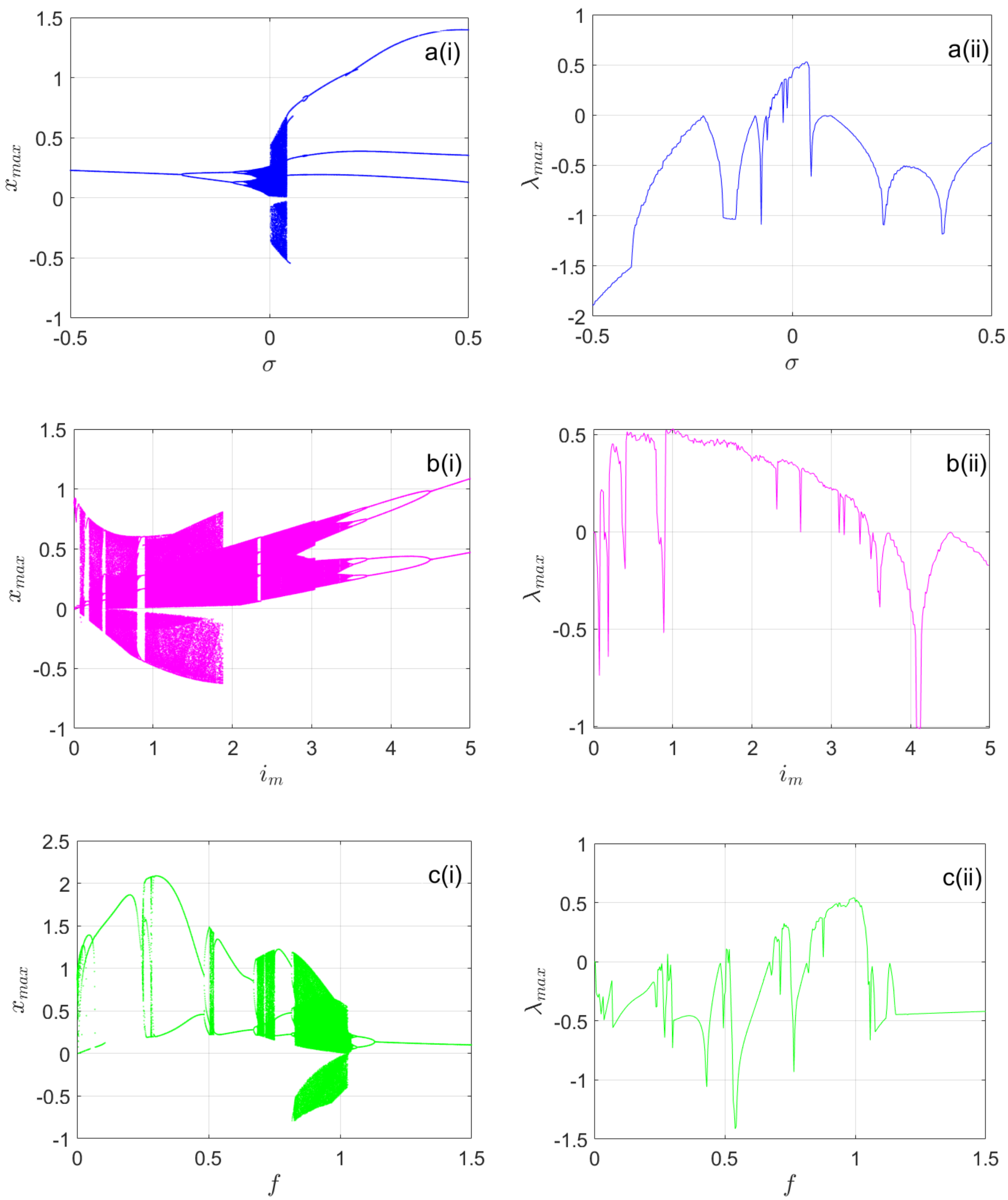

Fig.3: varieties of bifurcation diagrams (a(i), b(i), c(i)) with their related LLE (a(ii), b(ii), c(ii)). Diagrams in (a) are obtained for $i_m = 1$ and $f = 1$; diagrams in (b) are obtained for $\sigma = 0.03$ and $f = 1$ while diagrams in (c) are obtained for $\sigma = 0.03$ and $i_m = 1$. Initial starting points are those the previous charts based on upward continuation technique.

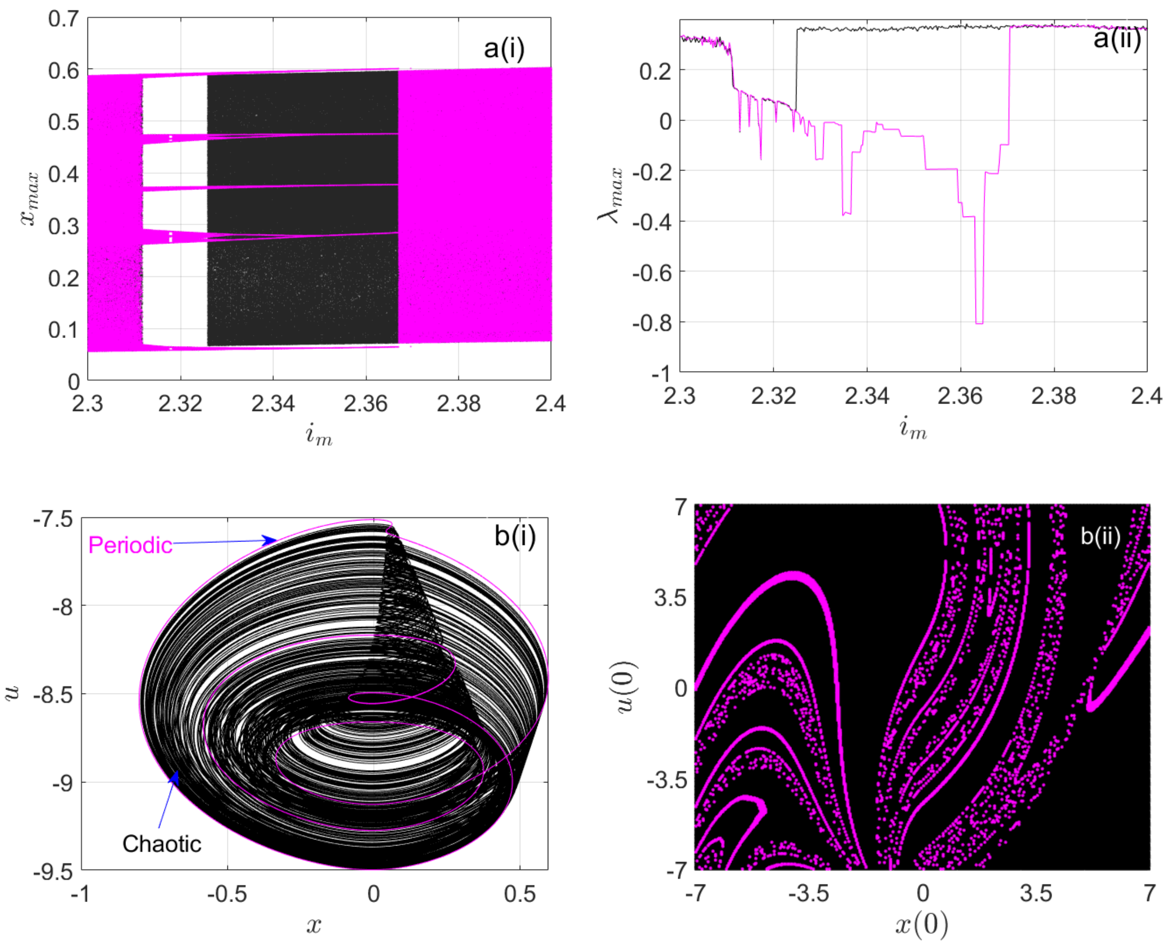

Fig.4: a(i) and a(ii) enlargement of the diagrams in Fig.2(b) obtained by increasing (magenta) respectively decreasing (black) the control parameter. The coexisting phase portraits in (b) are obtained for a value of the amplitude of the external excitation $i_m = 2.35$ with the initial starting points $(-4.62, -2.52)$ for the periodic behavior (magenta) and $(-1.9, -7)$ for the chaotic behavior (black).

These two regimes are able to exhibit firing activities of the chaotic and periodic nature, as can be seen by the bifurcation diagram in Fig. 3a(i) and the associated maximum Lyapunov exponent in Fig. 3a(ii). In the same line, a variety of self-excited firing activities can be captured when either amplitude i_m or frequency f are varied on the bifurcation diagrams in Fig. 3b (i) and Fig. 3c (i) and their related Lyapunov exponents plots in Fig. 3b(ii) and Fig. 3c(ii). Realizing and enlarging a portion of the diagrams of Fig. 3b in Figs. 4a(i) and 4a(ii), a window of hysteretic dynamics in which the model develops the coexistence of the chaotic and periodic firing activities is recorded. The mentioned coexisting attractors are presented using the phase portraits in Fig. 4b(i) with their related attraction basin in Fig. 4b(ii). From that attraction basin, it is clear that the probability of having a chaotic firing pattern (black region) is higher than that of having a periodic pattern (magenta region), which justifies the difficulty of capturing the periodic coexisting patterns from the electronic circuit realization of the neuron model.

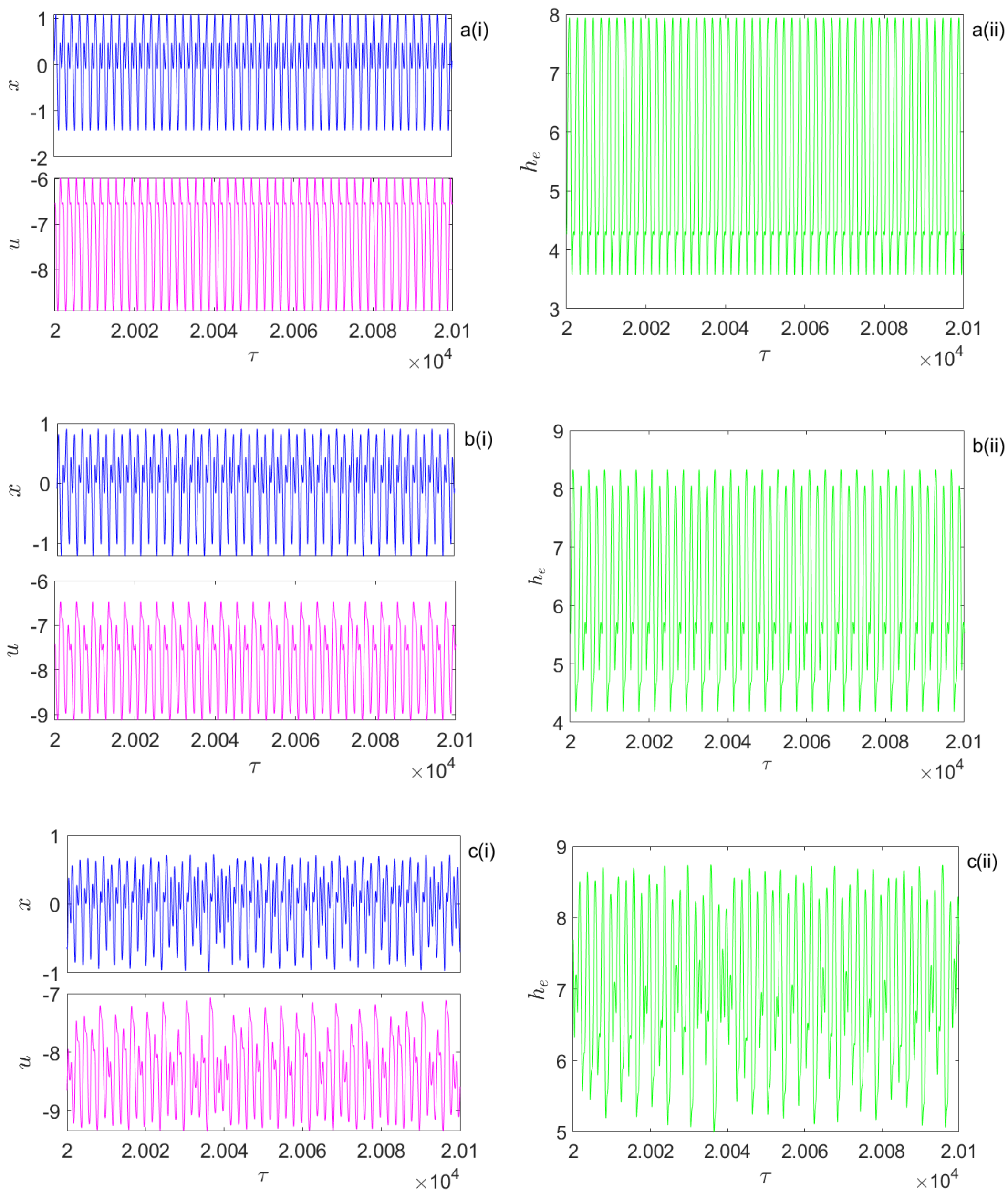

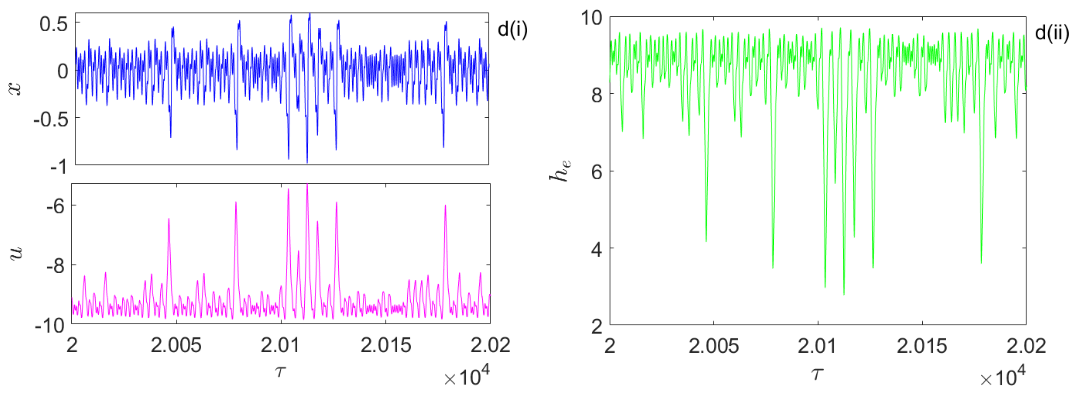

Fig.5: time series of the membrane potential (blue) and the recovery current (magenta) in the Left panel with their related energy consumption in the right panel. They are obtained for $i_m = 5$, (b) is obtained for $i_m = 4$, (c) is obtained for $i_m = 3$ while (d) is obtained for $i_m = 1$.

3.3 Energy related to the activity of the model

The energy function of the Rulkov neuron model can be estimated from the energy of the neuron's membrane potential and the energy of its ion channels. These terms are used to describe the dynamics of the neuron and how it responds to inputs from other neurons or the environment. In the Rulkov neuron model, energy is important in understanding how such systems evolve over time. Fig. 5 shows on the left-hand side the time evolution of the membrane potential (blue) and the ion channels (magenta) with their related energy on the right-hand side. As it can be seen from Figs. 5a to 5d, the density of the spikes on the energy graph is also proportional to the density of the spikes on membrane potential and ion channels. From the time evolution of the energy function reported in Fig. 5 (right-hand side), the contributions of the energy of the membrane potential and ion channels are analyzed through Fig. 6. In Fig. 6, the energy contribution of the ion channel is always greater than that of the membrane potential. For the value of the amplitude of the external simulation $i_m = 5$ to get the total energy function, the membrane potential contributed at 5%, while the ions channel contributed at 95%. While continuously decreasing the value of that amplitude, the contribution of the ion channel increases until it reaches 100%, while that of the membrane potential decreases until it reaches 0%.

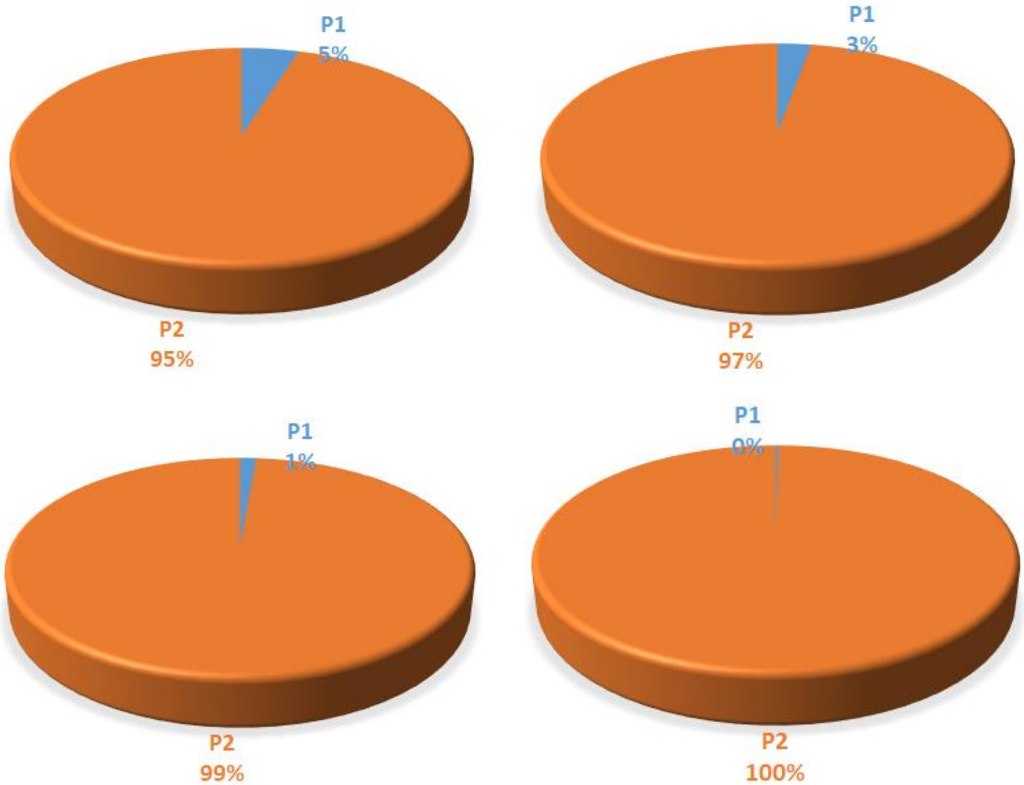

Fig.6: Energy contribution of the membrane potential and the ions channels during the various firing activities if Fig.5.

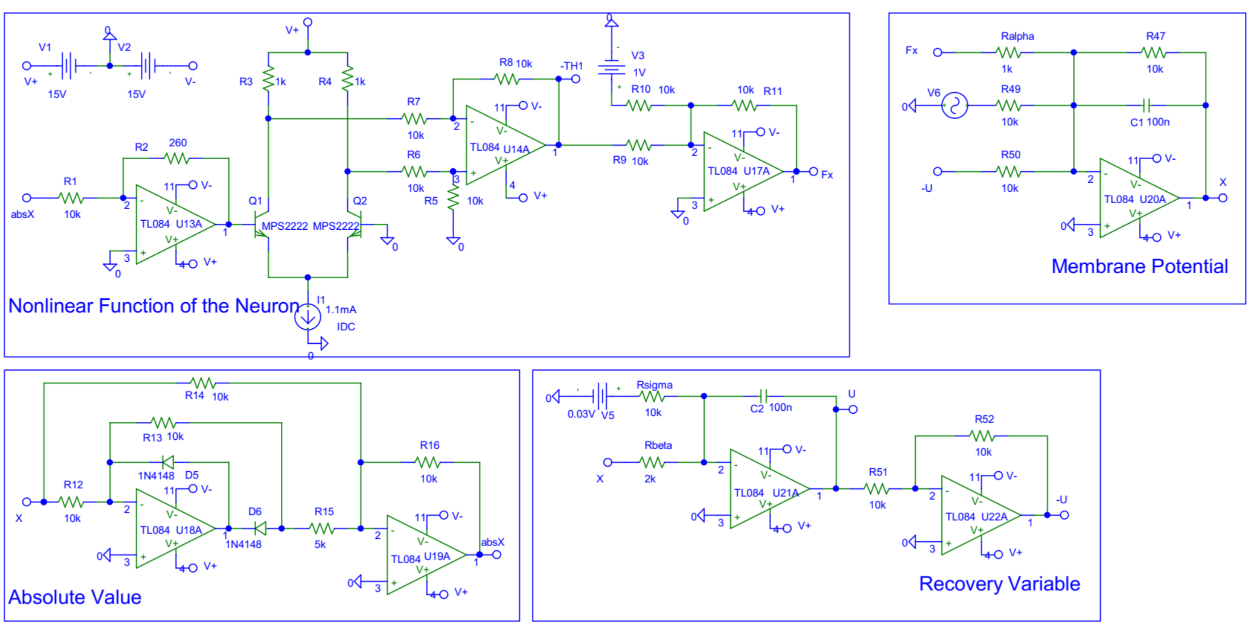

Fig.7: Circuit implementation of the proposed neuron model

4. Circuit validation and application of the model

4.1 design of the neural circuit

Circuit implementation represents an alternative approach to investigating the improved Rulkov presented in Eq. (1). Therefore, the circuit of a neuron model, such as the Rulkov neuron, has a key role in the development of the behavior and function of neurons in the brain. It allows researchers to study and simulate the electrical activity and dynamics of individual neurons, as well as the interactions between neurons in neural networks. In this particular contribution, the circuit of the neuron model is built in the PSpice simulation based on a constructed analog computer of the model. That analog computer equivalent is based on some discrete electrical components such as operational amplifiers, resistors, capacitors, transistors, diodes, DC and AC voltage sources, as well as a symmetric power supply. As it can be seen in Fig. 7, the circuit of the Rulkov neuron is made up of four main blocs, namely: the nonlinear activation function, which realizes the inverting summation between the tangent hyperbolic function (made up of a current source of $1.1mA$) and a constant DC source [25]; the absolute value function [26]. the membrane potential as the recovery variable for the ion current in the simulated neuron, The state equations associated with that neural circuit are provided in Eq. (11).

$$\begin{cases} C_1 \dfrac{dX}{dt} = \dfrac{1}{R_\alpha}\left(-\tanh\left(\dfrac{R_2}{2R_1V_T}|X|\right) + \dfrac{R_{11}}{R_{10}}V_3\right) - \dfrac{X}{R_{47}} + \dfrac{U}{R_{50}} + \dfrac{V_6}{R_{49}}\sin(2\pi F t) \\ C_2 \dfrac{dU}{dt} = -\dfrac{X}{R_\beta} - \dfrac{V_5}{R_\sigma} \end{cases} \tag{11}$$

Adopting the following variables changes $t = \tau RC$ with $R = 10k\Omega$, $C = 100nF$, $X = x \times 1V$, $U = u \times 1V$, $V_T = 26mV$, the circuit equations (Eq.11) are related to the dimensionless Equation of the model using the following relation:

$$C_1 = C_2 = C, \frac{R_2}{2R_1V_T} = 0.5, \quad \frac{R_{11}}{R_{10}} = 1, \qquad \frac{R}{R_\alpha} = \alpha \quad , \quad \frac{R}{R_\beta} = \beta, \quad \frac{RV_5}{1V \times R_\sigma} = \sigma \quad , \quad \frac{RV_6}{1V \times R_{49}} = \mathrm{I}_m \quad ,$$

$$RC \times F = f, \ \frac{R}{R_{47}} = \frac{R}{R_{50}} = 1 \tag{12}$$

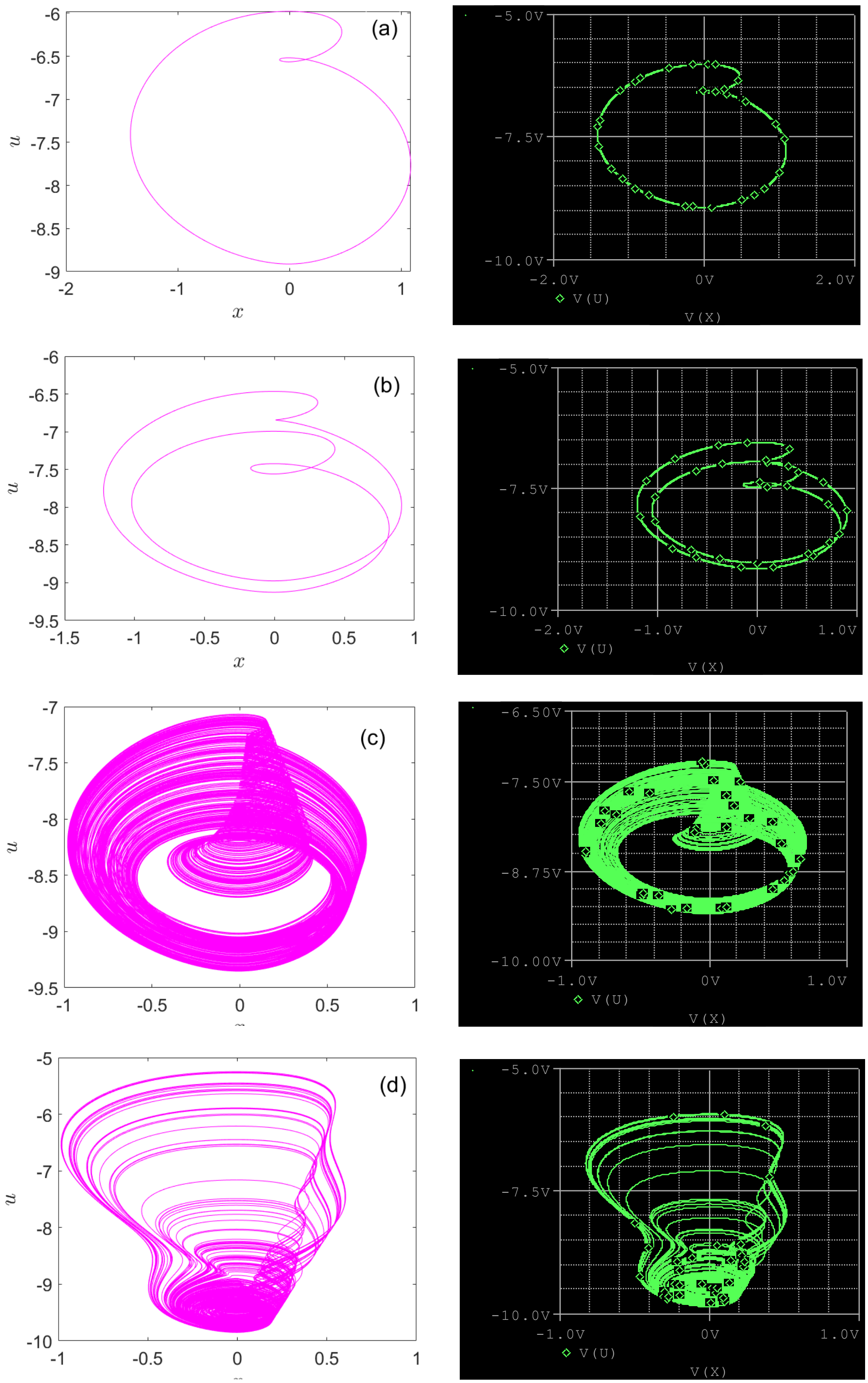
(a)
u
x
-6
-6.5
-7
-7.5
-8
-8.5
-9
-2
-1
0
1
-5.0V
-7.5V
-10.0V
-2.0V
0V
2.0V
V(U)
V(X)
(b)
u
x
-6
-6.5
-7
-7.5
-8
-8.5
-9
-9.5
-1.5
-1
-0.5
0
0.5
1
-5.0V
-7.5V
-10.0V
-2.0V
-1.0V
0V
1.0V
V(U)
V(X)
(c)
u
-7
-7.5
-8
-8.5
-9
-9.5
-1
-0.5
0
0.5
1
-6.50V
-7.50V
-8.75V
-10.00V
-1.0V
0V
1.0V
V(U)
V(X)
(d)
u
-5
-6
-7
-8
-9
-10
-1
-0.5
0
0.5
1
-5.0V
-7.5V
-10.0V
-1.0V
0V
1.0V
V(U)
V(X)

Fig.8: Phase space projection showing the correspondence between the numerical phase portraits and those obtained from the circuit implementation of the neuron model. (a) is obtained for $i_m = 5$ $(V_6 = 5V)$, (b) is obtained for $i_m = 4$ $(V_6 = 4V)$, (c) is obtained for $i_m = 3$ $(V_6 = 3V)$ while (d) is obtained for $i_m = 1$ $(V_6 = 1V)$. For the circuit simulations initial conditions are $(-7V, -5V)$ using the frequency $F = 1000 Hz$.

When varying the amplitude of the external source of the circuit, Fig. 8 is obtained using the same set of parameters that gives Fig. 5. On the left-hand side are the numerical phase portraits obtained from the direct integrations of the model given in Eq. (1), while on the right-hand side are the phase portraits obtained from the circuit realization of the neural model. From that result, it is obvious that the circuit of the neural model is able to reproduce most of the complex behaviors (varying from periodic to chaotic patterns) generated by the improved Rulkov neuron model.

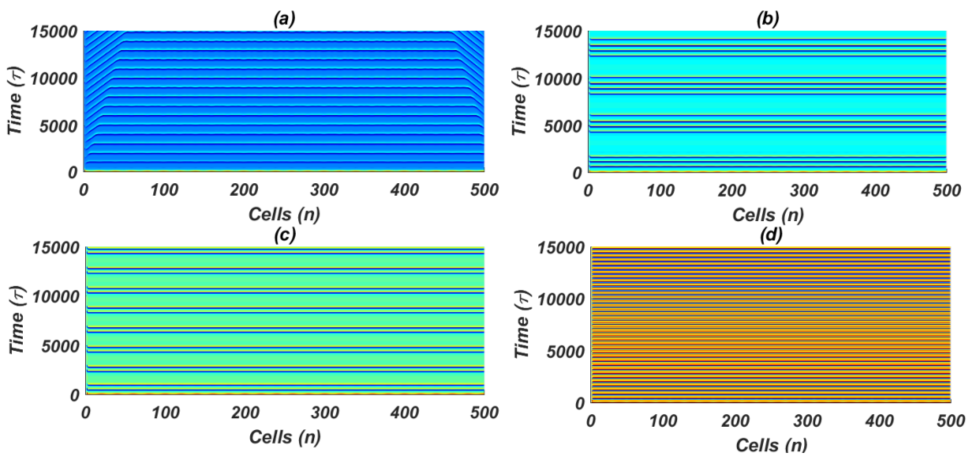

Fig.9: Spatiotemporal patterns of membrane potential calculated for 500 neurons over a transient period of 15000 time units for different values of f; (a) $f = 0.001$, (b) $f = 0.05$; (c) $f = 0.1$, (d) $f = 1$ with $I_m = 5.8$.

4.2 Information patterns in coupled Rulkov neurons

Apart the dynamics in electrical activity of a single neuron discussed above, we present the collective dynamics in information patterns of 500 coupled Rulkov neurons. Each neuron within the network is coupled with two nearest neighbors by an electrical coupling facilitated by gap junction synapses with coupling intensity K. This chain network of N neurons described by:

$$\begin{cases} \dot{x}_n = \alpha\left(-\tanh\left(0.5\left|x_n\right|\right)+1\right) - x_n + u_n + I_m \sin\left(2\pi f \tau\right) + K\left(x_{n+1} - x_n\right) + K\left(x_{n-1} - x_n\right) \\ \dot{u}_n = -\beta x_n - \sigma \end{cases} \quad (13)$$

with x_n describing the transmembrane action potential. The index n describes the position of a neuron within the network. Eq. (13) is integrated numerically by making use of the fourth-order Runge kulta computational scheme. We consider periodic boundary conditions and step size $\Delta t = 10^{-2}$. Weakly modulated plane waves having amplitudes $(0.1, 2)$, respectively are selected as initial conditions with wave number $q = 0.1\pi$ and perturbed wave number $Q = 0.1\pi$. We employed a transient period of 1.5×10^4 time units and plotted and showed spatiotemporal information patterns and time series for transmembrane action potential for various frequency values f. Figures 9 (a)-(c) and 10 (a)-(c) show the developed information benchmarks.

The Rulkov network lattice presents repetitive regular stripes of bright and dark bands which are almost periodic and localized in space and time. We remind that the bright regions correspond where neurons fire while in the dark regions, the neurons are quiescent. The grouped regular stripes in Figs. 9(b)-(c) predict bursting activities. The corresponding time series are plotted and presented in Figs. 10(a)-(c).

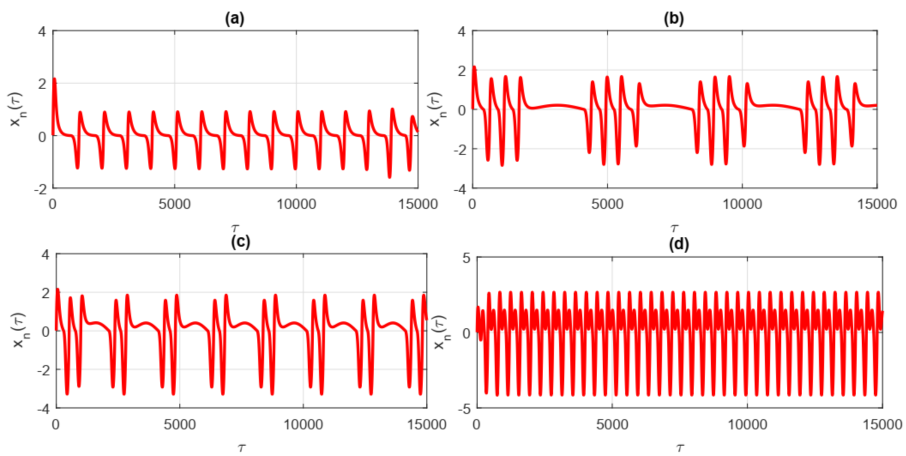

Fig.10: Time series of membrane potential calculated for 500 neurons over a transient period of 15000 time units for different values of f; (a) $f = 0.001$, (b) $f = 0.05$; (c) $f = 0.1$, (*d*) $f = 1$ with $I_m = 5.8$.

Figs.10(b)-(c) confirms the predicted bursting activities predicted in Figs.9(b)-(c) as the network presents diverse firing patterns including bursting states with different periods f is increased. The pattern dependence on f corroborates with relevant scientific reports in the domain of computational neuroscience [5, 27-29].

5. Conclusion

In this contribution, an improved Rulkov neuron model has been introduced and investigated. Using a two-parameter chart, a demarcation region showing the windows in the model display either stable or unstable dynamics has been computed. Based on the two-parameter Lyapunov exponent graphs, the global behavior of the considered model has been highlighted in terms of windows of periodic and chaotic patterns. Using bifurcation diagrams with their related graphs of the maximum Lyapunov, the variety of complex behaviors involving self-excited and hidden dynamics are investigated depending on the range of the parameters selected. Using the well-known Helmholtz theorem, the Hamilton energy that was used for the determination of the proportion of the energy of the ion channel and the membrane potential. From that proportional analysis, it was found that the contribution of the ion channel was always greater than that of the membrane potential for each value of the amplitude of the external current. From the circuit design of the neural, the results of the simulation of the patterns were in good accord with those obtained from the mathematical model. Using the chain network of 500 Rulkov neurons, an application to information patterns exploits initial conditions selected as slightly modulated plane waves. As a result, it was found that the Rulkov network lattice was able to present repetitive, regular stripes of bright and dark bands that were almost periodic and localized in space and time.

References

1. Gansel, K.S., *Neural synchrony in cortical networks: mechanisms and implications for neural information processing and coding.* Frontiers in Integrative Neuroscience, 2022. **16**: p. 900715.
2. Njitacke, Z.T., et al., *Dynamics of a memristive FitzHugh–Rinzel neuron model: application to information patterns.* The European Physical Journal Plus, 2023. **138**(5): p. 473.
3. Johansson, Y. and M. Ketzef, *Sensory processing in external globus pallidus neurons.* Cell Reports, 2023. **42**(1).
4. Takembo, C.N., H.P.E. Fouda, and T.C. Kofane, *Modulational instability in chain diffusive neuronal networks under electric field.* Indian Journal of Physics, 2023. **97**(2): p. 379-387.
5. Nyifeh, P., et al., *Unstable wave patterns of information in neural network under light illumination and magnetic field.* International Journal of Modern Physics B, 2023: p. 2450200.

6. Wagemakers, A. and M.A. Sanjuán, *Electronic circuit implementation of the chaotic Rulkov neuron model.* Journal of the Franklin Institute, 2013. **350**(10): p. 2901-2910.
7. Bashkirtseva, I., *Stochastic phenomena in one-dimensional Rulkov model of neuronal dynamics.* Discrete Dynamics in Nature and Society, 2015. **2015**.
8. Li, K., et al., *Memristive Rulkov neuron model with magnetic induction effects.* IEEE Transactions on Industrial Informatics, 2021. **18**(3): p. 1726-1736.
9. Bao, H., et al., *Memristive effects on an improved discrete Rulkov neuron model.* Science China Technological Sciences, 2023: p. 1-11.
10. Ma, M.-L., et al., *Synchronization coexistence in a Rulkov neural network based on locally active discrete memristor.* Chinese Physics B, 2023. **32**(5): p. 058701.
11. Xu, Q., et al., *Continuous non-autonomous memristive Rulkov model with extreme multistability.* Chinese Physics B, 2021. **30**(12): p. 128702.
12. Zhang, S., et al., *A multiplier-free Rulkov neuron under memristive electromagnetic induction: Dynamics analysis, energy calculation, and circuit implementation.* Chaos: An Interdisciplinary Journal of Nonlinear Science, 2023. **33**(8).
13. Xu, Q., et al., *Dynamical analysis of an improved FitzHugh-Nagumo neuron model with multiplier-free implementation.* Nonlinear Dynamics, 2023. **111**(9): p. 8737-8749.
14. Chen, X., et al., *Memristor initial-offset boosting and its bifurcation mechanism in a memristive FitzHugh-Nagumo neuron model with hidden dynamics.* Chaos, Solitons & Fractals, 2023. **174**: p. 113836.
15. Nkounga, I.T., et al., *Generalized FitzHugh–Nagumo model with tristable dynamics: Deterministic and stochastic bifurcations.* Chaos, Solitons & Fractals, 2023. **175**: p. 114020.
16. Li, X., et al., *Energy dependence of synchronization mode transitions in the delay-coupled FitzHugh-Nagumo system driven by chaotic activity.* Cognitive Neurodynamics, 2023: p. 1-16.
17. Xie, Y., et al., *Estimate physical reliability in Hindmarsh-Rose neuron.* Physics Letters A, 2023. **464**: p. 128693.
18. Kanagaraj, S., et al., *Collective dynamics of a coupled Hindmarsh–Rose neurons with locally active memristor.* Biosystems, 2023. **232**: p. 105010.
19. Hajian, D.N., et al., *Dynamics of Hindmarsh-Rose neurons connected via adaptive memristive synapse.* Chinese Journal of Physics, 2023.
20. Yu, D., et al., *Filtering properties of Hodgkin–Huxley neuron on different time-scale signals.* Communications in Nonlinear Science and Numerical Simulation, 2023. **117**: p. 106894.
21. Fan, W., et al., *Firing activity in a simplified Hodgkin–Huxley circuit with memristive sodium and potassium ion channels.* The European Physical Journal Plus, 2023. **138**(9): p. 834.
22. Wu, F., X. Hu, and J. Ma, *Estimation of the effect of magnetic field on a memristive neuron.* Applied Mathematics and Computation, 2022. **432**: p. 127366.
23. Rulkov, N.F., *Modeling of spiking-bursting neural behavior using two-dimensional map.* Physical Review E, 2002. **65**(4): p. 041922.
24. Leutcho, G.D., L. Woodward, and F. Blanchard, *Nonlinear dynamics of a single-gap terahertz split-ring resonator under electromagnetic radiation.* Chaos: An Interdisciplinary Journal of Nonlinear Science, 2023. **33**(10).
25. Tan, Y. and C. Wang, *A simple locally active memristor and its application in HR neurons.* Chaos: An Interdisciplinary Journal of Nonlinear Science, 2020. **30**(5).
26. He, S., et al., *Analog circuit of a simplified Tent map and its application in sensor position optimization.* IEEE Transactions on Circuits and Systems II: Express Briefs, 2022. **70**(3): p. 885-888.
27. Takembo, C.N., *Information pattern stability in memristive Izhikevich neural networks.* Modern Physics Letters B, 2022. **36**(12): p. 2250021.
28. Takembo, C.N., et al., *Effect of electromagnetic radiation on the dynamics of spatiotemporal patterns in memristor-based neuronal network.* Nonlinear Dynamics, 2019. **95**: p. 1067-1078.
29. Njitacke, Z.T., et al., *An enhanced FitzHugh–Nagumo neuron circuit, microcontroller-based hardware implementation: Light illumination and magnetic field effects on information patterns.* Chaos, Solitons & Fractals, 2023. **167**: p. 113014.